Published in final edited form as:
Cancer Cell. 2013 October 14; 24(4): . doi:10.1016/j.ccr.2013.08.012.

An integrin-linked machinery of cytoskeletal regulation that enables experimental tumor initiation and metastatic colonization

Tsukasa Shibue[1,2], **Mary W. Brooks**[1,2], and **Robert A. Weinberg**[1,2,3,4]

[1]Whitehead Institute for Biomedical Research Cambridge, MA 02142, USA

[2]MIT Ludwig Center for Molecular Oncology Cambridge, MA 02139, USA

[3]Department of Biology, Massachusetts Institute of Technology Cambridge, MA 02139, USA

Summary

Recently extravasated metastatic cancer cells employ the Rif/mDia2 actin-nucleating/polymerizing machinery in order to extend integrin β_1-containing, filopodium-like protrusions (FLPs), which enable them to interact productively with the surrounding extracellular matrix; this process governs the initial proliferation of these cancer cells. Here we identify the signaling pathway governing FLP lifetime, which involves integrin-linked kinase (ILK) and β-parvin, two integrin:actin-bridging proteins, that block cofilin-mediated actin-filament severing. Importantly, the combined actions of Rif/mDia2 and ILK/β-parvin/cofilin pathways on FLPs are required not only for metastatic outgrowth but also for primary tumor formation following experimental implantation. This provides one mechanistic explanation for how the epithelial-mesenchymal transition (EMT) program imparts tumor-initiating powers to carcinoma cells, since it enhances FLP formation through the activation of ILK/β-parvin/cofilin pathway.

Introduction

The great majority of disseminated cancer cells fail to survive and proliferate after landing in a foreign tissue (Chambers et al., 2002). This explains why only a small minority of disseminated cancer cells succeeds, via the process of colonization, in generating the macroscopic metastases that are responsible for more than 90% of cancer-associated deaths (Fidler, 2003). This highlights the need to elucidate the mechanisms that allow metastasized cells to survive and proliferate after settling in the parenchyma of foreign tissues.

We and others previously studied a set of three mouse mammary carcinoma cell lines – D2.0R, D2.1 and D2A1 (hereafter collectively referred to as D2 cells) – with differing metastatic potentials (Barkan et al., 2008; Shibue and Weinberg, 2009). Thus, after being introduced into mice via the tail vein, these three cell populations extravasate into the lung parenchyma with equal efficiency and exhibit comparable rates of initial survival; however, while the colonization-competent D2A1 cells subsequently proliferate rapidly, the colonization-deficient D2.0R and D2.1 cells fail to do so (see Figure S1A). Hence, these

[4]To whom correspondence should be addressed weinberg@wi.mit.edu, Tel: 617-258-5159, Fax: 617-258-5213.

three D2 cell populations provide a model system to study the mechanisms governing the proliferation of recently extravasated cancer cells in the lung parenchyma.

These studies led us to discover that focal adhesion kinase (FAK) signaling governs the post-extravasation proliferation of the aggressive D2A1 cells in the lungs, doing so by controlling the activity of the extracellular-signal regulated kinases (ERKs) (Shibue and Weinberg, 2009; Shibue et al., 2012). FAK activation in these D2A1 cells appeared to depend, in turn, on the interactions of these cells with components of the extracellular matrix (ECM) in the lung parenchyma, which are mediated specifically by the formation of elongated, integrin β_1-containing adhesion plaques. We found that the development of such plaques require the prior assembly of integrin β_1-containing, filopodium-like protrusions (FLPs) – actin-rich protrusions morphologically resembling filopodia formed by cells growing in monolayer culture. In contrast, the slowly-proliferating D2.0R and D2.1 cells develop very few FLPs and elongated adhesion plaques in the lung parenchyma and display low levels of FAK and ERK activation (Shibue et al., 2012; Figure S1A).

By testing various breast cancer cell lines that exhibit differing metastatic powers in mice, we also found that a diverse array of colonization-competent cells assemble such FLPs in far greater numbers than do their colonization-deficient counterparts (Shibue et al., 2012). This suggested that the ability to extend abundant FLPs critically determines the competence of these breast cancer cells to colonize foreign tissues. In the present study, we undertook to identify the key regulators of FLP formation with anticipation that these regulators also serve as molecular determinants of colonization competence.

Results

Differing expression levels of β-parvin in colonization-competent and -deficient cells

In an attempt to elucidate the mechanism(s) governing FLP formation, we exploited a three-dimensional (3D) culture model, termed “Matrigel on-top” (MoT), in which cells are plated above a layer of 100% Matrigel and then covered with culture medium containing 2% Matrigel (Debnath et al., 2003). When propagated in this MoT model, the aggressive D2A1 cells displayed abundant FLPs, while the nonaggressive D2.0R and D2.1 cells failed to do so; this mirrored the *in vivo* behaviors of these various cell types in the lung parenchyma (Shibue et al., 2012; Figures S1A, S1B).

In order to identify the mechanistic basis of differing FLP abundance observed in the MoT cultures, we tested the kinetics of FLP assembly and disassembly by time-lapse imaging. We found that the rate of *de novo* FLP formation was not noticeably different among these three D2 cell types (Figure 1A). In contrast, they exhibited a profound difference in the lifetime of FLPs: more than 60% of FLPs observed in the aggressive D2A1 cells persisted for more than 6 hours, while the majority (> 75%) of FLPs formed in the nonaggressive D2.0R and D2.1 cells persisted less than 90 minutes (Figure 1A, Movies S1–S3). This indicated that the difference in FLP abundance between these cell types could be attributed largely to the differing lifetimes of FLPs.

We proceeded to identify the molecular machinery governing FLP lifetime. In previous work, we found that the FLPs formed by the aggressive D2A1 cells in MoT culture displayed the β_1 subunit of integrins along the lengths of their shafts (Shibue et al., 2012). We also noted that others had demonstrated the critical role of integrin-ECM ligation in controlling local actin dynamics (Geiger et al., 2001). Together, these observations led us to speculate that the engagement of β_1-subunit-containing integrins with their ECM ligands along the lengths of FLP shafts governs the persistence of actin fibers that structurally support FLPs, thereby controlling FLP lifetime. Consistent with this speculation, the

knockdown of integrin β_1 expression in the D2A1 cells significantly reduced the lifetime, as well as the steady-state numbers, of FLPs formed by these cells (Figure S1C). In contrast, the knockdown of integrin β_1 expression in the poorly-FLPdisplaying D2.0R and D2.1 cells did not noticeably reduce either the abundance or lifetime of FLPs (Figure S1D).

Nonetheless, the short-lived FLPs that are naturally formed by these two indolent cell types, like those extended by the aggressive D2A1 cells, harbored integrin β_1 along their shafts, as demonstrated by use of an active-conformation specific antibody 9EG7 (Lenter et al., 1993; Figure S1E). We concluded that integrin β_1 was actively involved in the adhesions to ECM occurring along the shafts of FLPs in all the three types of D2 cells, regardless of the persistence time of their FLPs. It appeared, therefore, that integrin β_1-mediated adhesions contributed critically to the prolonged lifetime of FLPs in the aggressive D2A1 cells, doing so by increasing the persistence of actin filaments that formed the core of these protrusions, whereas formation of these adhesions did not appear to affect the stability of the FLPs in the indolent D2.0R and D2.1 cells.

Based on this thinking, we examined the mechanisms connecting integrin β_1-mediated adhesions with the actin fibers that structurally support FLPs. In particular, we addressed the roles of integrin:actin-linking proteins, which are thought to govern the coordination between the integrin-mediated adhesions and the control of actin organization in the vicinity of these adhesions (Geiger et al., 2001). To begin, we measured the abundance of mRNAs encoding 23 known linker proteins. Among these, the mRNA encoding β-parvin stood out, since its levels were approximately 100-fold higher in the aggressive D2A1 cells than in the other two indolent D2 cell types. In contrast, none of the other 22 mRNAs surveyed exhibited more than a 2.2-fold difference in expression levels in the D2A1 cells relative to the mean expression levels in the indolent D2.0R and D2.1 cells (Figure 1B).

As expected from mRNA expression, the expression of β-parvin protein could be detected by immunoblotting only in the aggressive D2A1 cells (Figure 1C). Moreover, the knockdown of β-parvin expression by 87–94% in the D2A1 cells caused a 51–56% decrease in FLP abundance as well as a significant reduction of FLP lifetime (Figures 1D, 1E, S1F, Movies S4, S5). In addition, the knockdown of the expression of integrin-linked kinase (ILK), an essential linker between β-parvin and integrin β chains (Yamaji et al., 2001; Figure 2A), also reduced the number of FLPs in the D2A1 cells (Figure 1D). Conversely, ectopic β-parvin expression in the more indolent D2.0R and D2.1 cells extended FLP lifetime and increased the steady-state number of these protrusions, an effect that could be blunted by concomitant ILK knockdown (Figures S1F–H, Movies S6, S7). Hence, the differences in the lifetime and thus abundance of FLPs observed in the various D2 cell types were attributable, at least in part, to the differing expression levels of β-parvin, which appeared to control FLP lifetime in an ILK-dependent manner.

βPIX/Cdc42/PAK axis as an effector of ILK/β-parvin in controlling FLP formation

Given the key role played by β-parvin in the regulation of FLPs, we sought to uncover the role of other proteins beyond ILK that might collaborate with β-parvin in this process. In fact, in addition to serving as a physical link between integrins and the actin cytoskeleton, β-parvin is known to play a regulatory role in the cytoskeleton by interacting with αPIX and βPIX (PAK-interacting exchange factors) (Rosenberger et al., 2003). Both PIX proteins recruit and then activate Cdc42 and Rac1 GTPases, which in turn proceed to activate the Group I class of p21-activated kinases (PAKs), i.e., PAK1-3, thereby regulating cytoskeletal organization (Figure 2A; Bokoch, 2003).

We therefore determined whether PIX/Cdc42(Rac)/PAK signaling contributes to the β-parvin-dependent process of FLP regulation. Immunoprecipitation analysis revealed that β-

parvin expressed in the aggressive D2A1 cells interacted physically with βPIX, the only PIX isoform expressed at a detectable level in these cells (Figures 2B, S2F). Moreover, the knockdown of βPIX expression (by 98–99%) resulted in a 46–66% decrease in the number of FLPs formed by the MoT-cultured D2A1 cells (Figures 2C, S2A), indicating that β-parvin cooperates with βPIX in regulating FLP abundance.

We proceeded to examine the role of β-parvin in driving the signaling events downstream of βPIX, namely, the sequential activation of Cdc42 (Rac1) and PAK1-3. The knockdown of β-parvin expression in the D2A1 cells grown in MoT culture reduced the levels of GTP-bound, active Cdc42 and Rac1 by 70–88% and 57–78%, respectively (Figures 2D, S2B). This was accompanied by the reduced phosphorylation of PAK1 at residues critical to its kinase activity – threonine 423 (T^{423}) within its catalytic domain as well as serines 199 and 204 ($S^{199/204}$) within its autoinhibitory domain (Figure 2E). Conversely, β-parvin overexpression in the MoT-cultured, otherwise-indolent D2.0R and D2.1 cells elevated the levels of active Cdc42 and Rac1 and augmented phosphorylation of PAK1 on T^{423} and $S^{199/204}$ (Figures 2D, 2E, S2B). Hence, in these D2 carcinoma cell types, β-parvin expression was both necessary and sufficient for activating Cdc42, Rac1 and PAKs when these cells were growing in MoT cultures.

We also compared the roles of Cdc42 and Rac1 as downstream effectors of the β-parvin/βPIX complex and found that Cdc42 knockdown reduced both PAK1 phosphorylation and FLP abundance far more efficiently than did Rac1 knockdown (Figures 2E, S2C, S2D; Shibue et al., 2012). This indicated that Cdc42, rather than Rac1, serves as a key intermediary in the β-parvin/βPIX-dependent PAK activation.

Finally, we tested the involvement of PAKs in FLP regulation. The inhibition of PAK activity by overexpressing a dominant-negative PAK1-AID fragment, which inhibits all the three of PAK1-3 (Zhao et al., 1998), resulted in a 47% reduction in the number of FLPs formed by the D2A1 cells in MoT culture (Figure 3A). Conversely, overexpression of a constitutively active PAK1 mutant (PAK1 L107F) in the D2.0R and D2.1 cells increased the number of FLPs by 3.2- and 3.0-fold, respectively (Figure 3A). Together, these observations demonstrated the critical role of the ILK/β-parvin/βPIX/Cdc42/PAK signaling axis in supporting abundant FLP display (see Figure 3B).

LIMK/cofilin axis as a downstream mediator of the effect of PAKs on FLPs

The work described above did not reveal how PAKs control FLP abundance. However, we noted that earlier studies had implicated the presence of multiple effector pathways contributing to the PAK-dependent control of cytoskeletal organization (Bokoch, 2003; Figure 3B). Thus, PAKs activate LIM domain kinases (LIMKs), which in turn inactivate the ADF/cofilin family of proteins (i.e., ADF, cofilin1 and cofilin2; hereafter referred to collectively as cofilin), the central regulators of actin filament severing. Independent of this, PAKs also impair actomyosin contractility by inactivating myosin light-chain kinase (MLCK), thereby reducing the phosphorylation level of the regulatory myosin light chain (rMLC) (see Figure 2A).

We undertook to specify the role(s) of PAKs in FLP regulation. In the MoT-cultured, aggressive D2A1 cells, the inhibition of PAK activity, achieved either by β-parvin knockdown or PAK1-AID overexpression, impaired the phosphorylation of cofilin1 on serine 3 (S^3), an inhibitory modification usually catalyzed by the PAK-effector LIMKs (Yang et al., 1998; Figure 2F). In contrast, neither of these manipulations noticeably affected rMLC phosphorylation on serine 19, which is catalyzed by another PAK-effector, MLCK (Figure 2F). Hence, between the two effector pathways of PAKs (Figure 2A), the LIMK/

cofilin pathway, but not the MLCK/rMLC pathway, was controlled by the ILK/β-parvin/βPIX/Cdc42/PAK signaling in these cells.

Consistent with this notion, FLP formation in the MoT-cultured D2A1 cells was impaired by overexpression of a constitutively active cofilin1 mutant (cofilin1 S3A; Moriyama et al., 1996; Figure 3A). Moreover, the overexpression of either β-parvin or the constitutively active mutant of either PAK1 or LIMK1 (PAK1 L107F and LIMK1-Kd3, respectively) enabled the nonaggressive D2.1 cells to extend far more FLPs (2.4–2.7-fold increase in FLP number), while failing to do so when the constitutively-active cofilin1 S3A mutant was expressed concomitantly (Figure 3C). Collectively, these observations indicated that ILK/β-parvin/βPIX/Cdc42/PAK signaling contributes to the display of abundant FLPs largely, if not entirely, by causing LIMK-dependent cofilin inactivation, which protects the actin spine of FLPs from cofilin-mediated cleavage, thereby resulting in the increased persistence of FLPs (Figure 3B).

Two signaling pathways that cooperatively govern FLP formation

The ILK/β-parvin/βPIX/Cdc42/PAK/LIMK/cofilin (hereafter referred to as 'ILK/β-parvin/cofilin') signaling axis characterized above was not the only determinant of FLP abundance. In earlier work, we had uncovered the essential contribution of the Rif/mDia2 actin-nucleating/polymerizing machinery to FLP formation (Shibue et al., 2012). Indeed, others had shown that Rif and mDia2 cooperatively induce the nucleation of actin monomers and subsequent elongation of actin filaments (Mellor, 2010), which comprise the structural core of FLPs. These earlier observations, together with the presently demonstrated contribution of cofilin-inactivating signaling pathway to FLP abundance, suggested that there are actually two distinct signaling pathways – Rif/mDia2 signaling on the one hand and ILK/β-parvin/cofilin signaling on the other – that collaborate in the induction and/ maintenance of FLPs (Figure 3B). Thus, the first pathway causes the formation of actin fibers that drives the initial extension of FLPs, while the second pathway ensures the stabilization of these FLPs once they are formed.

We undertook to study in detail the cooperative actions of these two signaling axes. We found that changes in FLP abundance induced by the enforced activation of Rif/mDia2 signaling were not associated with noticeable alterations in the cofilin1 phosphorylation on S^3, the site critical to the regulation of cofilin1 activity (Figures 2F, 3C). This contrasted sharply with the regulation of FLPs by ILK/β-parvin/cofilin signaling, which involved and depended critically on changes in cofilin activity (Figures 2F, 3C). Together, these observations indicated the independent, complementary actions of these two signaling pathways in regulating FLP abundance (Figure 3B).

We also analyzed the effect of simultaneously manipulating both pathways. Here we found that the enhanced display of FLPs in the naturally poorly-FLP-forming D2.1 cells, which could be achieved by the enforced activation of ILK/β-parvin/cofilin signaling, was reversed by the concomitant knockdown of either Rif or mDia2 expression (Figure 3D). This indicated that the tonic activity of Rif/mDia2 signaling is naturally maintained in the D2.1 cells and suggested that the inability of these cells to display abundant FLPs could be ascribed largely to their ineffective activation of ILK/β-parvin/cofilin signaling, which resulted in turn from their failure to synthesize significant levels of β-parvin protein (Figure 1C).

We proceeded further to examine the kinetics of FLP assembly and disassembly by time-lapse imaging. Consistent with the effects of β-parvin in extending the lifetime of FLPs (Figures 1E, S1G), inhibition of ILK/β-parvin/cofilin signaling in the aggressive D2A1 cells, achieved by the expression of either dominant-negative PAK1-AID fragment or

constitutively active cofilin1 S3A mutant, reduced the persistence period of FLPs, while the enforced activation of this signaling in the indolent D2.1 cells increased this persistence (Figures 3E, 3F). However, none of these manipulations noticeably affected the rate of *de novo* FLP formation. In contrast, the enforced elevation of Rif/mDia2 signaling activity in the indolent D2.1 cells resulted in a significant (≥ 1.9-fold) increase in the rate of FLP initiation and a modest extension of FLP lifetime (Figure 3F, Movies S6, S8).

These observations reinforced the notion that Rif/mDia2 signaling contributes primarily to the *de novo* formation of FLPs by stimulating the nucleation/polymerization of the actin fibers that structurally support FLPs, while ILK/β-parvin/cofilin signaling specifically helps to maintain the resulting FLPs by suppressing the cofilin-dependent cleavage of such actin fibers. Together, these two signaling collaborate to enable cells to display large numbers of FLPs (see Figure 3B).

ILK/β-parvin/cofilin signaling and *in vitro* cell behavior

As mentioned above, we had found that the formation of FLPs contributes to the assembly of integrin β_1-containing, mature adhesion plaques of elongated morphology in cells grown in MoT culture, doing so by fostering the nucleation of protein complexes that comprise the core of these plaques (Figure 4A; Shibue et al., 2012). Consistent with this earlier observation, the inhibition of ILK/β-parvin/cofilin signaling – the signaling axis critical to the extended lifetime and thus to the display of abundant FLPs – reduced the number of integrin β_1-containing adhesion plaques in the D2A1 cells growing in MoT culture (Figures 4B, S4A). In addition, the inhibition of ILK/β-parvin/cofilin signaling reduced the levels of activation-associated phosphorylation of FAK and ERKs and attenuated proliferation when the D2A1 cells were growing under MoT culture conditions, while not noticeably affecting their proliferation in monolayer culture (Figures 4C–E, S4B–D). This reinforced the role of FLP formation as a critical trigger for the establishment of cell-matrix adhesions and rapid cell proliferation in cells grown in MoT culture (see Figure 4A).

We proceeded to test whether the contribution of ILK/β-parvin/cofilin signaling to these processes was generalizable to other cancer cell types. In fact, our previous work had demonstrated that, among 18 different lines of human breast cancer cells, those that were competent to form metastatic colonies developed far more abundant FLPs than did their colonization-deficient counterparts (Shibue et al., 2012). The subsequently pursued time-lapse observations of such cells growing in MoT culture revealed that the FLPs formed in the colonization-competent BT549, MDA-MB-231 and SUM1315 cells persisted far longer than those extended by the colonization-deficient BT474, SK-BR-3, T47D and ZR-75-1 cells (Figure 1F). Consistently, these three colonization-competent cell types exhibited elevated activity of the FLP-stabilizing ILK/β-parvin/cofilin signaling, as determined by examining the levels of cofilin1 phosphorylation on S^3 – the endpoint of this signaling pathway (see Figure 3B), relative to the four colonization-deficient cell types tested here (Figures S2E, S2F). Together, these observations supported the notion that the display of abundant FLPs, observed specifically in the colonization-competent cells, is attributable, in part, to the elevated activity of the ILK/β-parvin/cofilin signaling and the resulting prolonged lifetime of FLPs.

We also blocked the activity of ILK/β-parvin/cofilin signaling in the colonization-competent SUM159 and MDA-MB-231 human breast cancer cells. This resulted in impaired FLP formation and reduced proliferation rate in MoT cultures, while minimally affecting their proliferation in monolayer (2D) cultures (Figures S3A, 4F). Hence, ILK/β-parvin/cofilin signaling contributed critically to the abundant FLP display and rapid cell proliferation in the 3D MoT cultures of multiple colonization-competent carcinoma cell types.

ILK/β-parvin/cofilin signaling and metastatic aggressiveness *in vivo*

The MoT culture used in the experiments cited above was designed to approximate the microenvironment surrounding cancer cells that have recently extravasated into the lung parenchyma (Barkan et al., 2008; Shibue and Weinberg, 2009). We wished to extend the findings of these experiments by determining whether the ILK/β-parvin/cofilin signaling axis also regulates metastatic cell behaviors in the lungs. In fact, various strategies to block this signaling pathway all reduced (by 2.3- to 9.0-fold) the number of macroscopic lung metastases formed 24 days after the tail-vein injection of the D2A1 cells; this was associated with impaired proliferation within the lung tissue as measured 7 days after the injection (Figures 5A, S5A). In contrast, none of these manipulations noticeably affected D2A1 cell proliferation in monolayer culture (Figure 4C).

We also examined in detail lung sections prepared 10 days after tail-vein injection of the D2A1 cells. Here again, the inhibition of ILK/β-parvin/cofilin signaling in the D2A1 cells decreased (2.3- to 4.1-fold) the numbers of large metastatic colonies (those with > 20 cells/colony), while the numbers of small colonies (≤ 20 cells/colony), which consisted largely of viable but nonproliferative cells, were actually increased (1.3- to 2.4-fold; Figures 5B, S5B). This echoed the previously-observed effect of knocking down Rif or mDia2 expression in the D2A1 cells (Shibue et al., 2012). Together, these observations led us to conclude that blocking FLP formation in the recently extravasated D2A1 cells constrains these cells to reside in the lung parenchyma as viable, weakly-proliferating micrometastatic cells.

We undertook to analyze how the inhibition of ILK/β-parvin/cofilin signaling affects the initial steps of extravasation and post-extravasation processes of metastasis. In fact, the blockade of this signaling axis in the aggressive D2A1 cells did not noticeably affect the efficiency of extravasation into the lung parenchyma, while being effective in reducing the abundance of FLPs and mature adhesion plaques formed by the extravasated cells; this was accompanied by a reduced level of FAK activation relative to that of the control cells (Figures 5C, 5D, S5C–E). Hence, the action of ILK/β-parvin/cofilin signaling was critical, following extravasation into the lung parenchyma, to the FLP-dependent establishment of productive cell-matrix interactions by the D2A1 cells, which in turn governed their subsequent proliferation (see Figure 4A).

We asked whether other types of colonization-competent cells also depend on the activity of ILK/β-parvin/cofilin signaling in order to colonize the lung tissue. Accordingly, we tested three colonization-competent mouse cell types, namely, TS/A mammary carcinoma cells, B16F10 melanoma cells and TRAMP-C2 prostate cancer cells, all of which exhibited β-parvin-dependent FLP formation in MoT culture (Figures 1G, S1I). We found that, in all three cases, the knockdown of β-parvin expression reduced the number of macroscopic lung metastases formed after tail-vein injection (Figures 5E, S5F). Similarly, blockade of ILK/β-parvin/cofilin signaling in the human breast cancer cell lines SUM159 and MDA-MB-231 also impaired formation of lung macrometastases by these cells (Figure 5F). Notably, none of these manipulations discernibly affected the proliferation of these cells in monolayer cultures (Figures 4F, S4E). These observations confirmed the role of ILK/β-parvin/cofilin signaling as a critical controller of metastatic aggressiveness in multiple cancer cell types.

FLP formation and tumorigenicity of orthotopically-implanted cells

These various observations caused us to test the involvement of ILK/β-parvin/cofilin signaling in earlier steps of experimental tumor formation. Thus, we speculated that the adaptations that experimentally implanted cancer cells must initially undergo in sites of engraftment resemble those that are required for the establishment of disseminated cancer cells as founders in sites of metastatic colonization. Based on this thinking, we implanted

various cancer cell types into either orthotopic (mammary fat pads in the case of mammary carcinomas) or ectopic subcutaneous sites in murine hosts, doing so with or without manipulating these cells by blocking ILK/β-parvin/cofilin signaling. This revealed that some of these manipulations reduced the incidence of primary tumor formation: for example, the knockdown of βPIX expression reduced tumor incidence following the implantation of the D2A1 cells in the mammary fat pad from 96% to 42–64% (Figure S6AC). This echoed our previous observation that inhibition of Rif/mDia2 signaling in the D2A1 cells reduced the rate of primary tumor formation after the orthotopic implantation (Shibue et al., 2012). Together, these observations suggested that the ability of cells to display abundant FLPs contributes to the establishment of primary tumors at sites of implantation.

We pursued these effects further by measuring tumor-initiating frequency of two cancer cell types, namely D2A1 and MDA-MB-231 cells, after implanting them at limiting dilutions. We found that blocking FLP formation, achieved by inhibiting either the Rif/mDia2 or ILK/β-parvin/cofilin pathway, significantly reduced the estimated frequency of tumor-initiating cells (TICs) in both cell populations (Figures 6A, S6D). This led us speculate that the formation of FLPs, which enables rapid proliferation of cancer cells following extravasation into the lung parenchyma (see Figure 4A), also governs the initial proliferation of cancer cells at sites of implantation, thereby critically affecting the efficiency with which these cells establish primary tumors in host mice.

Indeed, shortly after implantation into mammary fat pads, the D2A1 cells displayed FLPs, which resembled those formed by these cells following extravasation into the lung parenchyma (Figures 6B, 6C). Moreover, the number of FLPs formed 2 days after the implantation of the D2A1 cells was decreased by blocking either the Rif/mDia2 or ILK/β-parvin/cofilin signaling pathway, which was accompanied by the significant reduction of the proliferation rate that was measured 3 days later (Figures 6D, 6E). Hence, the cooperative actions of Rif/mDia2 and ILK/β-parvin/cofilin signaling pathways and the resulting, abundant formation of FLPs (see Figure 3B) contributed critically to the active proliferation of recently implanted D2A1 cells within mammary fat pads.

We also found that both Rif- and β-parvin-knockdown impaired FAK activation in the orthotopically implanted D2A1 cells (Figure 6F). This attenuation of FAK signaling was likely to account for the reduced TIC frequency caused by these knockdowns, since the concomitant expression of the constitutively-active CD2-FAK fusion protein partially restored this frequency (Figure 6G). In addition, the knockdown of FAK expression impaired ERK activation in the mammary fat pad-implanted D2A1 cells (Figure 6F). Together, these observations indicated that the proliferation of the recently implanted cancer cells in the mammary fat pads is governed, in part, by the mechanisms involving FLP extension and the resulting activation of FAK/ERK signaling, which mirrored the regulation on the proliferation of recently extravasated cancer cells in the lungs (see Figure 4A).

Correlation between ILK/β-parvin/cofilin signaling activity and tumorigenic potential

We examined in greater detail the behavior of the D2A1 cells that had been recently implanted into the mammary fat pads. This revealed that the numbers of FLPs formed by the individual cells within the D2A1 cell population was highly variable from one cell to another (Figure S6E), which led us to speculate that the cells displaying more abundant FLPs had a higher tumor-initiating potential, i.e., an ability to seed tumors in host mice following implantation, than did those forming only small numbers of these protrusions. To test this, we fractionated the D2A1 cells into different subpopulations in order to examine whether the FLP-forming ability of the cells in these various subpopulations correlated with their content of TICs.

Others have separated mouse mammary carcinoma cells based on the expression of CD29 and CD24 cell surface markers and found that the subpopulation of cells with $CD29^{high}$/$CD24^{high}$ (29H/24H) profile exhibited a significant enrichment of TICs (Zhang et al., 2008). Consistent with this observation, we noted that the 29H/24H fraction of the D2A1 cells exhibited a 4.1- and 27-fold higher TIC frequency than did the $CD29^{high}$/$CD24^{low}$ (29H/24L) and $CD29^{low}$ (29L) groups, respectively (Figures 7A, 7B). We also found that cells of the aggressive 29H/24H subpopulation extended a larger number of FLPs than did the cells of the other two subpopulations both in MoT culture and within the mammary fat pads (Figures 7C, 7D, S7A). Hence, the observed difference in the TIC frequency of these various D2A1 cell subpopulations correlated with the FLP-forming abilities of their constituent cells.

Wishing to extend these observations to other cell types, we studied the HMLER transformed human mammary epithelial cells (Elenbaas et al., 2001). As reported previously, these HMLER cells can be sorted, according to the expression profile of the CD44 and CD24 markers, into two subpopulations: a TIC-enriched $CD44^{high}$/$CD24^{low}$ (44H/24L) subpopulation and a TIC-depleted $CD44^{low}$/$CD24^{high}$ (44L/24H) subpopulation (Mani et al., 2008; Figure 7E). When propagated in MoT culture, cells of the 44H/24L subpopulation displayed a far larger (13.4×) number of FLPs than did cells of the 44L/24H subpopulation (Figure 7F). Hence, in both the D2A1 and HMLER cultures, the cells from the TIC-enriched subpopulations extended FLPs more abundantly than did the cells from the TIC-depleted subpopulations.

We undertook to identify the determinants of differing FLP abundance between the cells of these various subpopulations. Time-lapse observation of these cells growing in the MoT culture revealed that FLPs formed by cells of the TIC-enriched subpopulations (i.e., 29H/24H in the D2A1 cells and 44H/24L in the HMLER cells) exhibited significantly longer lifetime than those extending from cells of the corresponding other subpopulations (Figures S7C, S7D). Consistent with this observation, cells of these TIC-enriched subpopulations exhibited a higher level of the cofilin1-inactivating S^3 phosphorylation – the endpoint of the signaling pathway that governs FLP lifetime, i.e., ILK/β-parvin/cofilin signaling (see Figure 3B) – than did the cells of the other subpopulations (Figure 7G). Moreover, FLP formation by cells of the HMLER 44H/24L subpopulation was impaired by expressing the constitutively active cofilin1 S3A mutant in these cells, which ultimately reduced the TIC frequency in this subpopulation (Figures 7H, S7E, S7F). Collectively, these various observations supported the notion that the elevated TIC frequency – observed in the 29H/24H subpopulation of the D2A1 cells and the 44H/24L subpopulation of the HMLER cells – is attributable, in part, to the enhanced FLP-stabilizing ability of their constituent cells, which results, in turn, from the elevated activity in these cells of the ILK/β-parvin/cofilin signaling.

ILK/β-parvin/cofilin signaling and the process of epithelial-mesenchymal transition

Cancer cells can often develop a higher tumor-initiating potential during the course of tumor progression (Pece et al., 2010). In the case of carcinomas, this acquisition of malignant phenotypes is often achieved by the passage through the cell-biological program termed the epithelial-mesenchymal transition (EMT); moreover, as demonstrated previously, the forced induction of an EMT in cancer cells endows them with a greatly increased tumor-initiating potential (Mani et al., 2008; Morel et al., 2008).

These earlier observations, together with our present demonstration of the critical role of FLPs in the process of tumor initiation, prompted us to ask whether the EMT-dependent induction of the tumor-initiating potential involves and depends on the enhancement of FLP formation. Accordingly, we ectopically expressed the Twist transcription factor, an inducer

of the EMT program (Yang et al., 2004), in the naturally-epithelial HMLER cells (Figures 8A, 8B, S8A). Consistent with previous observations (Mani et al., 2008), Twist-induced EMT in these cells was accompanied by an enhanced tumor-initiating potential in the mammary fat pads (132-fold increase in TIC frequency) and an increased power of metastasis formation (Figures 8C, 8D).

Of relevance here, Twist-induced EMT in the HMLER cells stimulated their FLP-forming ability both in MoT culture and following orthotopic implantation, which was accompanied by marked increases in the expression levels of multiple components of the ILK/β-parvin/cofilin signaling, namely ILK (4.7×), β-parvin (13.6×) and LIMK1 (3.2×) (Figures 8B, 8E, 8F). Moreover, both the elevated expression of these three components of the ILK/β-parvin/cofilin signaling pathway and the enhanced display of FLPs were reproduced by other strategies of EMT induction, specifically the overexpression of Snail transcription factor and the knockdown of E-cadherin adhesion protein (Figures 8B, 8E).

We proceeded to examine the functional role of the elevated β-parvin expression on the behavior of Twist-expressing HMLER cells. This revealed that the knockdown of β-parvin expression partially reversed multiple properties conferred on these cells by the expression of Twist, including increased FLP abundance and elevated phosphorylation levels of PAK1 (on T^{423} and $S^{199/204}$) and cofilin1 (on S^{3}), all of which were observed in MoT culture (Figures 8B, 8E, 8F, S8B). Moreover, β-parvin knockdown also reduced the aggressiveness of HMLER-Twist cells *in vivo*: both tumor initiation and metastasis formation were impaired significantly by this knockdown (Figures 8C, 8D). We concluded that the elevated tumor-initiating and metastasis-forming powers imparted to the HMLER cells by Twist-induced EMT, and presumably by the EMTs induced by other strategies, depended on enhanced FLP display; this was enabled, in turn, by the elevated expression levels of several components of ILK/β-parvin/cofilin signaling pathway including β-parvin.

We also tested whether the connection between FLP formation and EMT process could be extended to other cell types. Accordingly, we induced an MET (mesenchymal-epithelial transition) – the reverse process of EMT – in the naturally mesenchymal D2A1 cells, doing so by the combination of Snail knockdown and E-cadherin overexpression (Figures 8B, S8C–F). As anticipated, the D2A1 cells that underwent an MET exhibited a profound loss of tumor-initiating and metastasis-forming powers (Figures 8C, 8D). Moreover, this MET induction was associated with the 2.7-fold decrease in the number of FLPs formed by these cells in MoT culture (Figure S8G). In addition, the D2A1 cells that underwent an MET also exhibited decreased expression of several components of the ILK/β-parvin/cofilin signaling pathway, namely, ILK, β-parvin and LIMK1, all of which contrasted to the effects of EMT in the HMLER cells (Figures 8B, S8H). Hence, in both HMLER cells and the D2A1 cells, the transition between the epithelial and mesenchymal states involved changes in the expression levels of multiple components of the ILK/β-parvin/cofilin signaling pathway. This altered, in turn, their ability to form FLPs and ultimately contributed to changes in tumor-initiating and metastasis-forming powers exhibited by the cells undergoing this cell state transition.

Discussion

While the role of integrin-mediated cell-matrix adhesions in enabling the outgrowth of metastases had been recognized (Aguirre Ghiso et al., 1999; Barkan et al., 2008), the manner by which extravasated cancer cells interact with the ECM components of the parenchyma of their host tissue remained to be elucidated. We previously reported that the ability of cancer cells to form abundant FLPs following extravasation into the parenchyma of foreign tissues contributes critically to the establishment by these cells of productive interactions with the

ECM of their host tissue (Shibue et al., 2012). We also demonstrated the essential role of Rif/mDia2 actin-nucleating/polymerizing machinery in the formation of FLPs. Here we have described two findings that together provide an important extension to our understanding of the role of FLPs in controlling cancer cell behaviors.

To begin, we identified a signaling mechanism that yields an extended lifetime of FLPs and thereby contributes to the abundance of these protrusions in the colonizationcompetent cancer cells. Thus, the activation of the ILK/β-parvin/cofilin signaling axis at sites of FLP formation enables the persistence of these protrusions once they are assembled. As is the case with the Rif/mDia2 signaling (Shibue et al., 2012), the action of ILK/β-parvin/cofilin signaling is critical to the metastatic colony-forming ability of multiple aggressive cancer cell types.

Importantly, the enforced activation of this signaling pathway, on its own, does not always suffice to confer metastatic powers on otherwise-indolent cancer cells. For example, in the nonaggressive D2.1 cells, which do not express β-parvin at a detectable level, ectopic β-parvin expression sufficed to enable these cells to display abundant FLPs in MoT culture. However, these β-parvin-expressing D2.1 cells did not subsequently succeed in developing mature adhesion plaques and in proliferating rapidly under the MoT conditions, nor did they form a large number of macroscopic metastases in the lungs following tailvein injection (Figure S3). Hence, these D2.1 cells appeared to suffer one or more additional defect(s) beyond the lack of β-parvin expression that precluded their aggressive behavior both in MoT culture *in vitro* and within the lung parenchyma *in vivo*.

While not addressed directly by the present work, we suggest that the dynamics of FLP formation and the contribution of FLPs to metastatic outgrowth will prove to be relevant to the colonization process of various target tissues. Indeed, we previously demonstrated that blocking FLP formation by Rif knockdown in the B16F10 melanoma cells diminishes the ability of these cells to colonize multiple organs, such as the lungs, liver and bone marrow, following intracardiac injection into syngeneic mice (Shibue et al., 2012). This prompts us to suggest that FLP formation and resulting establishment of productive cell-matrix interactions represent a common prerequisite to the metastatic colonization of many types of target organs.

The second lesson of the present study relates to the role of FLPs in the establishment of primary tumors by experimentally implanted cancer cells. Thus, as shown here, multiple cancer cell types depend on the FLP-regulating signaling pathways for efficiently establishing primary tumors following experimental implantation in murine hosts. In support of this finding, we also presented examples where the increased tumor-initiating potential of cancer cells was correlated closely with their enhanced ability of FLP formation. More specifically, cells of the TIC-enriched subpopulations of both D2A1 and HMLER cells displayed FLPs far more abundantly than the remaining cells in these populations.

Recent studies have revealed that many types of solid tumors contain both cells that can efficiently seed tumors upon transplantation into mice and those that are unable to do so; these are often referred to as cancer stem cells (CSCs) and non-stem cancer cells (non-CSCs), respectively (Clevers, 2011). The efficient tumor seeding by many, if not all, types of carcinoma CSCs is likely to be supported by the EMT program. Indeed, the induction of EMT suffices to confer on cancer cells not only an increased tumor-initiating potential but also many other attributes of CSCs, including enhanced resistance to chemotherapeutic agents and a slower rate of proliferation (Gupta et al., 2009). However, the specific mechanism(s) by which the EMT program potentiates the tumor-initiating powers of carcinoma cells has remained elusive. The present observations point to the contribution of

the EMT program to increasing the expression of proteins that are critical for FLP formation, and to the role of FLP formation in governing tumor-initiating potential. Together, this provides a mechanistic explanation of how the EMT program can contribute to the elevated tumor-initiating ability of CSCs.

To summarize, we propose that in certain and perhaps many types of cancer cells, their initial proliferation following both experimental implantation and metastatic dissemination is governed, in part, by the common regulatory mechanism involving FLP formation and the resulting assembly of mature adhesion plaques. Clearly, other factors, such as cytokines, growth factors, and responsive stromal cells in the microenvironment, must also contribute to determining the eventual successful formation of both primary and metastatic tumors. Nonetheless, the initial formation of FLPs, which depends critically on the Rif/mDia2 and ILK/β-parvin/cofilin signaling pathways, appears to constitute a key rate-limiting step that governs both processes of tumor formation.

Experimental Procedures

Cell culture

The Matrigel on-top (MoT) culture was performed as described previously (Shibue and Weinberg, 2009). Unless otherwise indicated, cells were propagated for 12 hours (for FLP formation), 5 days (for adhesion and phosphorylation analyses) or 10 days (for cell number determination).

Animal procedure

All animal experiments conformed to the Guide for the Care and Use of Laboratory Animals published by the National Research Council and were approved by the MIT Committee on Animal Care.

Live-cell imaging

Live-cell imaging was performed on a spinning-disc confocal microscopy system, equipped with a Nikon Eclipse TE2000E inverted microscope.

Statistical analysis

Statistical analyses were carried out by Student's *t*-test, unless otherwise indicated.

Supplementary Material

Refer to Web version on PubMed Central for supplementary material.

Acknowledgments

We are grateful to FB Gertler and RO Hynes for advices; F Reinhardt, T Chavarria, M Griffin, E Vasile, P Wisniewski and W Zhang for assistance; AS Alberts, XR Bustelo, CJ Der, SP Ethier, R Fässler, PL Lollini, H Mellor, FR Miller, M Takeichi, RY Tsien, C Wu and D Yarar for reagents. T.S. received postdoctoral fellowships from Human Frontier Science Program, Japan Society for the Promotion of Science, and Ludwig Fund for Cancer Research. R.A.W. is an American Cancer Society research professor and a Daniel K. Ludwig Foundation cancer research professor. This work was funded by grants from Breast Cancer Research Foundation, National Institute of Health (P01 CA080111) and Ludwig Fund for Cancer Research.

References

Aguirre Ghiso JA, Kovalski K, Ossowski L. Tumor dormancy induced by downregulation of urokinase receptor in human carcinoma involves integrin and MAPK signaling. J Cell Biol. 1999; 147:89–104. [PubMed: 10508858]

Barkan D, Kleinman H, Simmons JL, Asmussen H, Kamaraju AK, Hoenorhoff MJ, Liu ZY, Costes SV, Cho EH, Lockett S, et al. Inhibition of metastatic outgrowth from single dormant tumor cells by targeting the cytoskeleton. Cancer Res. 2008; 68:6241–6250. [PubMed: 18676848]

Bokoch GM. Biology of the p21-activated kinases. Annu Rev Biochem. 2003; 72:743–781. [PubMed: 12676796]

Chambers AF, Groom AC, MacDonald IC. Dissemination and growth of cancer cells in metastatic sites. Nat Rev Cancer. 2002; 2:563–572. [PubMed: 12154349]

Clevers H. The cancer stem cell: premises, promises and challenges. Nat Med. 2011; 17:313–319. [PubMed: 21386835]

Debnath J, Muthuswamy SK, Brugge JS. Morphogenesis and oncogenesis of MCF-10A mammary epithelial acini grown in three-dimensional basement membrane cultures. Methods. 2003; 30:256–268. [PubMed: 12798140]

Elenbaas B, Spirio L, Koerner F, Fleming MD, Zimonjic DB, Donaher JL, Popescu NC, Hahn WC, Weinberg RA. Human breast cancer cells generated by oncogenic transformation of primary mammary epithelial cells. Genes Dev. 2001; 15:50–65. [PubMed: 11156605]

Fidler IJ. The pathogenesis of cancer metastasis: the 'seed and soil' hypothesis revisited. Nat Rev Cancer. 2003; 3:453–458. [PubMed: 12778135]

Geiger B, Bershadsky A, Pankov R, Yamada KM. Transmembrane crosstalk between the extracellular matrix--cytoskeleton crosstalk. Nat Rev Mol Cell Biol. 2001; 2:793–805. [PubMed: 11715046]

Gupta PB, Onder TT, Jiang G, Tao K, Kuperwasser C, Weinberg RA, Lander ES. Identification of selective inhibitors of cancer stem cells by high-throughput screening. Cell. 2009; 138:645–659. [PubMed: 19682730]

Lenter M, Uhlig H, Hamann A, Jeno P, Imhof B, Vestweber D. A monoclonal antibody against an activation epitope on mouse integrin chain beta 1 blocks adhesion of lymphocytes to the endothelial integrin alpha 6 beta 1. Proc Natl Acad Sci U S A. 1993; 90:9051–9055. [PubMed: 7692444]

Mani SA, Guo W, Liao MJ, Eaton EN, Ayyanan A, Zhou AY, Brooks M, Reinhard F, Zhang CC, Shipitsin M, et al. The epithelial-mesenchymal transition generates cells with properties of stem cells. Cell. 2008; 133:704–715. [PubMed: 18485877]

Matsuda C, Kameyama K, Tagawa K, Ogawa M, Suzuki A, Yamaji S, Okamoto H, Nishino I, Hayashi YK. Dysferlin interacts with affixin (beta-parvin) at the sarcolemma. J Neuropathol Exp Neurol. 2005; 64:334–340. [PubMed: 15835269]

Mellor H. The role of formins in filopodia formation. Biochim Biophys Acta. 2010; 1803:191–200. [PubMed: 19171166]

Morel AP, Lievre M, Thomas C, Hinkal G, Ansieau S, Puisieux A. Generation of breast cancer stem cells through epithelial-mesenchymal transition. PLoS One. 2008; 3:e2888. [PubMed: 18682804]

Moriyama K, Iida K, Yahara I. Phosphorylation of Ser-3 of cofilin regulates its essential function on actin. Genes Cells. 1996; 1:73–86. [PubMed: 9078368]

Pece S, Tosoni D, Confalonieri S, Mazzarol G, Vecchi M, Ronzoni S, Bernard L, Viale G, Pelicci PG, Di Fiore PP. Biological and molecular heterogeneity of breast cancers correlates with their cancer stem cell content. Cell. 2010; 140:62–73. [PubMed: 20074520]

Rosenberger G, Jantke I, Gal A, Kutsche K. Interaction of alphaPIX (ARHGEF6) with beta-parvin (PARVB) suggests an involvement of alphaPIX in integrin-mediated signaling. Hum Mol Genet. 2003; 12:155–167. [PubMed: 12499396]

Shibue T, Brooks MW, Inan MF, Reinhardt F, Weinberg RA. The outgrowth of micrometastases is enabled by the formation of filopodium-like protrusions. Cancer Discov. 2012; 2:706–721. [PubMed: 22609699]

Shibue T, Weinberg RA. Integrin beta1-focal adhesion kinase signaling directs the proliferation of metastatic cancer cells disseminated in the lungs. Proc Natl Acad Sci U S A. 2009; 106:10290–10295. [PubMed: 19502425]

Yamaji S, Suzuki A, Sugiyama Y, Koide Y, Yoshida M, Kanamori H, Mohri H, Ohno S, Ishigatsubo Y. A novel integrin-linked kinase-binding protein, affixin, is involved in the early stage of cell-substrate interaction. J Cell Biol. 2001; 153:1251–1264. [PubMed: 11402068]

Yang J, Mani SA, Donaher JL, Ramaswamy S, Itzykson RA, Come C, Savagner P, Gitelman I, Richardson A, Weinberg RA. Twist, a master regulator of morphogenesis, plays an essential role in tumor metastasis. Cell. 2004; 117:927–939. [PubMed: 15210113]

Yang N, Higuchi O, Ohashi K, Nagata K, Wada A, Kangawa K, Nishida E, Mizuno K. Cofilin phosphorylation by LIM-kinase 1 and its role in Rac-mediated actin reorganization. Nature. 1998; 393:809–812. [PubMed: 9655398]

Zhang M, Behbod F, Atkinson RL, Landis MD, Kittrell F, Edwards D, Medina D, Tsimelzon A, Hilsenbeck S, Green JE, et al. Identification of tumor-initiating cells in a p53-null mouse model of breast cancer. Cancer Res. 2008; 68:4674–4682. [PubMed: 18559513]

Zhao ZS, Manser E, Chen XQ, Chong C, Leung T, Lim L. A conserved negative regulatory region in alphaPAK: inhibition of PAK kinases reveals their morphological roles downstream of Cdc42 and Rac1. Mol Cell Biol. 1998; 18:2153–2163. [PubMed: 9528787]

Highlights

- Abundance of filopodium-like protrusions (FLPs) depends on their persistence periods.
- Integrin-actin linking proteins govern cofilin activity as well as FLP persistence.
- FLPs critically support both metastatic outgrowth and experimental tumor formation.
- Epithelial-mesenchymal transition (EMT) in carcinoma cells enhances FLP formation.

Significance

The proliferation of recently extravasated metastatic cancer cells and experimentally implanted cancer cells depends on their ability to establish integrin-mediated adhesions with the extracellular matrix of the tissues that they initially encounter. The formation of these adhesions is enabled by the extension of filopodium-like protrusions (FLPs), whose formation, in turn, is encouraged by the epithelial-mesenchymal transition (EMT) program. In this fashion, the EMT program facilitates proliferation of both recently extravasated metastatic carcinoma cells and those that are experimentally implanted. These dynamics help to explain how the EMT program can increase the tumor-initiating potential of carcinoma cells – the trait that is used experimentally to define cancer stem cells.

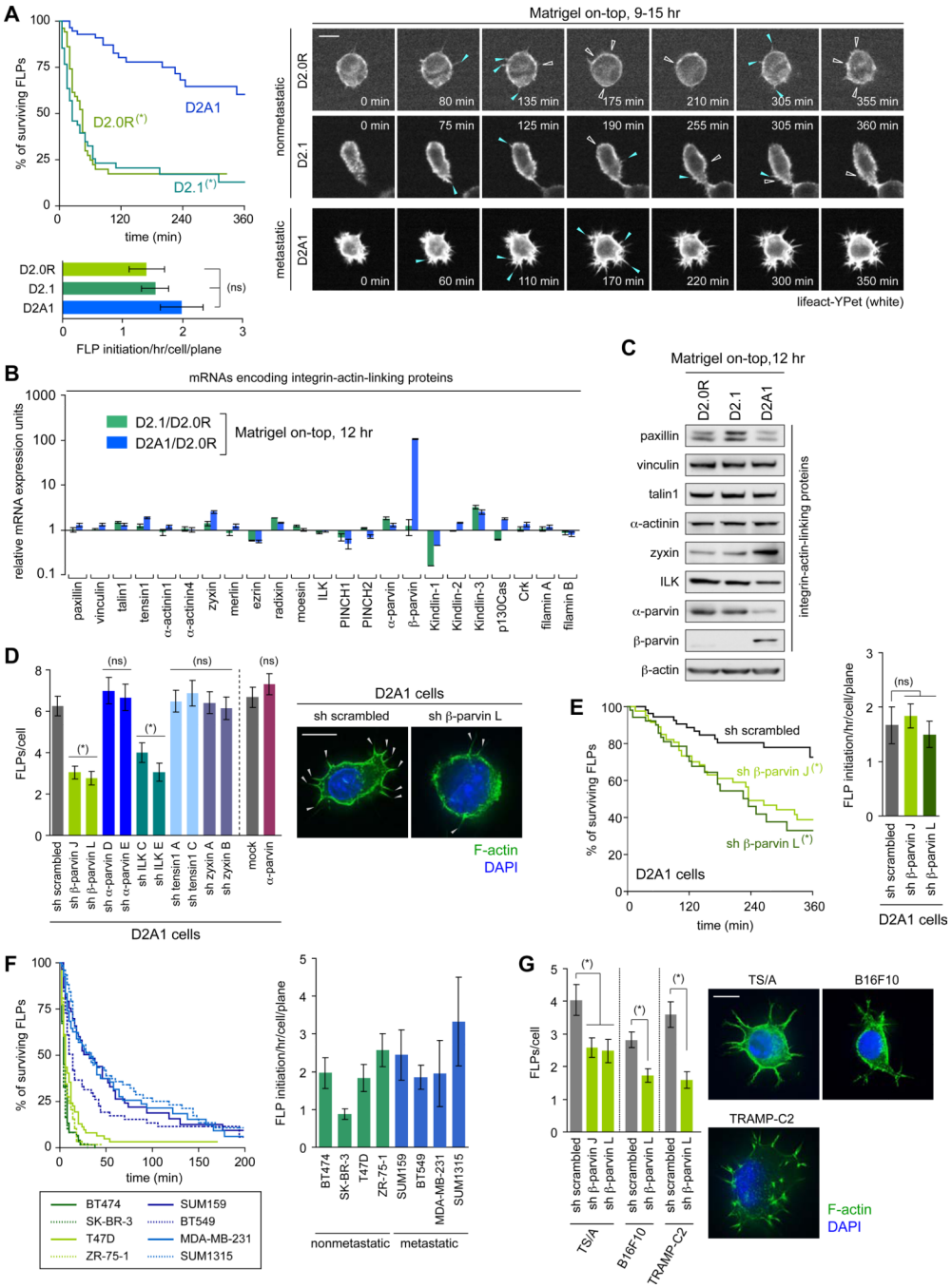

Figure 1. β-parvin as a key regulator of FLP formation

(A) Kinetics of FLP assembly and disassembly. Three different D2 cell populations (expressing an actin marker lifeact-YPet) were analyzed by time-lapse microscopy. The appearance of new FLPs and the retraction of previously-present FLPs are marked by blue and open-white arrowheads, respectively. The periods of FLP persistence (top-left) and the rate of *de novo* FLP formation (bottom-left) were plotted. See also Movies S1–S3.

(B, C) mRNA (B) and protein (C) expression for various integrin:actin-linkers.

(D) Role of ILK/β-parvin in FLP formation. D2A1 cells with knockdowns for various integrin:actin-linkers or overexpression of α-parvin were propagated in MoT cultures and

stained with phalloidin (F-actin; green) and DAPI (nuclei; blue) (right). The numbers of FLPs per cell were plotted (left). Knocking down the expression of β-parvin and ILK, but not the overexpression of α-parvin, reduced FLP abundance. Hence, the expression level of β-parvin, but not that of α-parvin, has a critical effect on FLP abundance.

(E) Contribution of β-parvin to the extended FLP lifetime. The D2A1 cells manipulated as indicated (also expressing lifeact-YPet) were analyzed as in A. See also Movies S4, S5.

(F) Persistence of FLPs formed by human breast cancer cells. Various human breast cancer cell lines (expressing lifeact-YPet) were analyzed by time-lapse microscopy for FLP persistence and the rate of *de novo* FLP formation.

(G) β-parvin-dependent FLP formation in various metastatic cell types. Three metastatic mouse cell types were analyzed for FLP formation in MoT cultures.

Values = means ± SD (n = 3: B) or means ± SEM ($n \geqq 20$: A, E, F; n = 100: D, G). Bars = 10 μm. In A and E, (*) $p < 0.002$ (by log-rank test; vs D2A1 in A, vs sh scrambled in E), (ns) $p > 0.1$. In D and G, (*) $p < 0.01$ (vs sh scrambled/mock), (ns) $p > 0.3$. See also Figure S1.

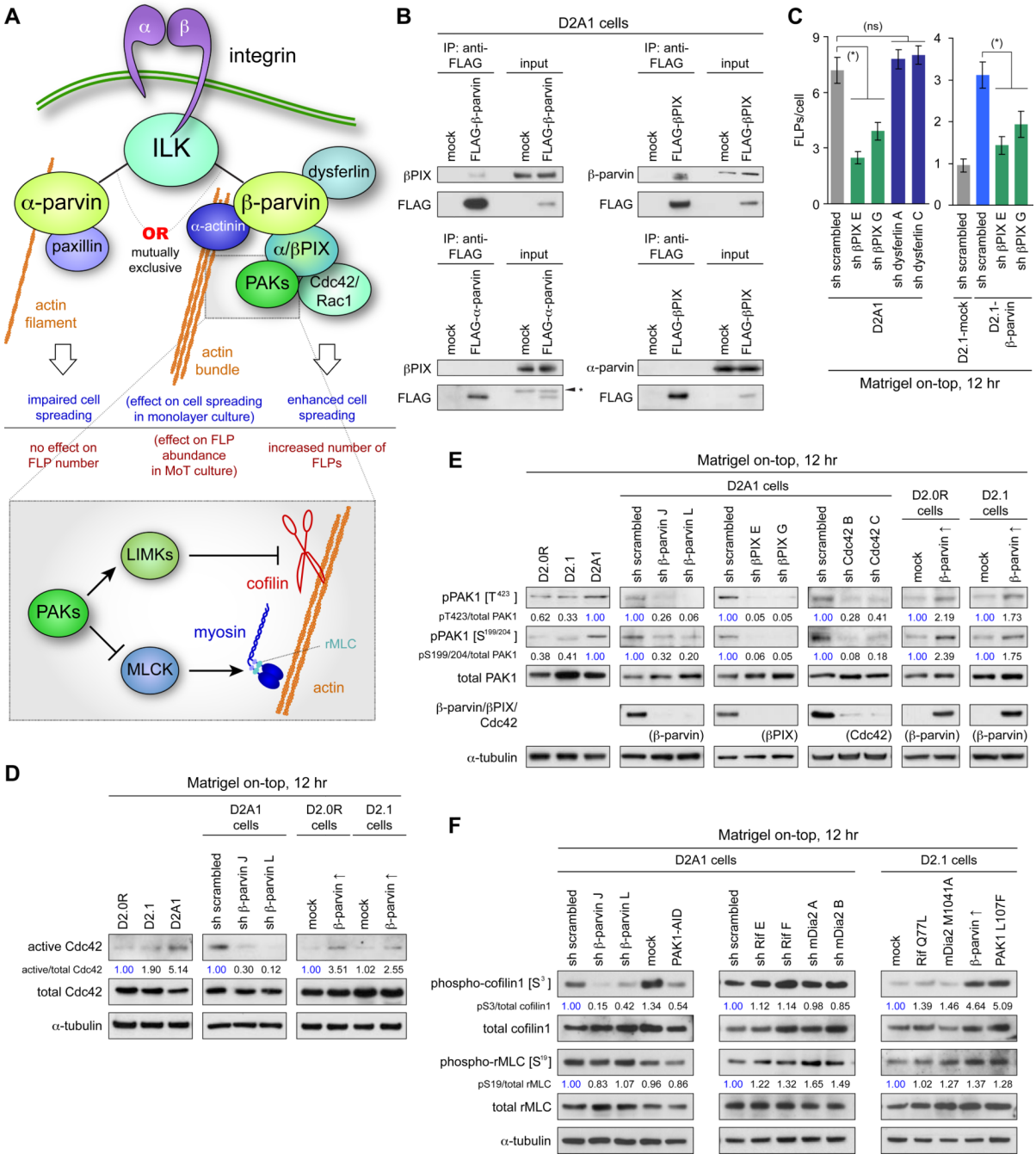

Figure 2. ILK/β-parvin/βPIX/Cdc42/PAK/LIMK/cofilin signaling in FLP formation

(A) Integrin-actin coupling by ILK/α-parvin and ILK/β-parvin complexes. α-parvin and β-parvin bind to ILK, each providing a link between integrins and actin cytoskeleton, while having different effects on cell behaviors.

(B) β-parvin/βPIX interactions. Lysates from FLAG-β-parvin-, FLAG-α-parvin- or FLAG-βPIX-expressing cells were subjected to anti-FLAG immunoprecipitation and analyzed by immunoblotting. βPIX interacts with β-parvin, but not with α-parvin. (*) nonspecific bands.

(C) Role of βPIX in FLP regulation. Knocking down the expression of βPIX, but not that of dysferlin (a transmembrane protein that interacts with β-parvin; Matsuda et al., 2005)

reduced FLP abundance in the D2A1 cells. Values = means ± SEM (*n* = 100). (*) $p < 0.001$, (ns) $p > 0.3$.

(D) β-parvin expression and Cdc42 activation. Values represent the intensities of the active Cdc42 bands relative to that of corresponding total Cdc42 band.

(E) β-parvin/Cdc42/βPIX signaling in PAK phosphorylation. Here and in F, values represent the intensities of pPAK1 (phospho-cofilin1/phospho-rMLC) bands relative to that of the corresponding total PAK1 (cofilin1/rMLC) band. The blots are representative of multiple independent experiments.

(F) Cofilin and rMLC phosphorylation in the downstream of β-parvin/PAK signaling. Bars = 10 μm. See also Figure S2.

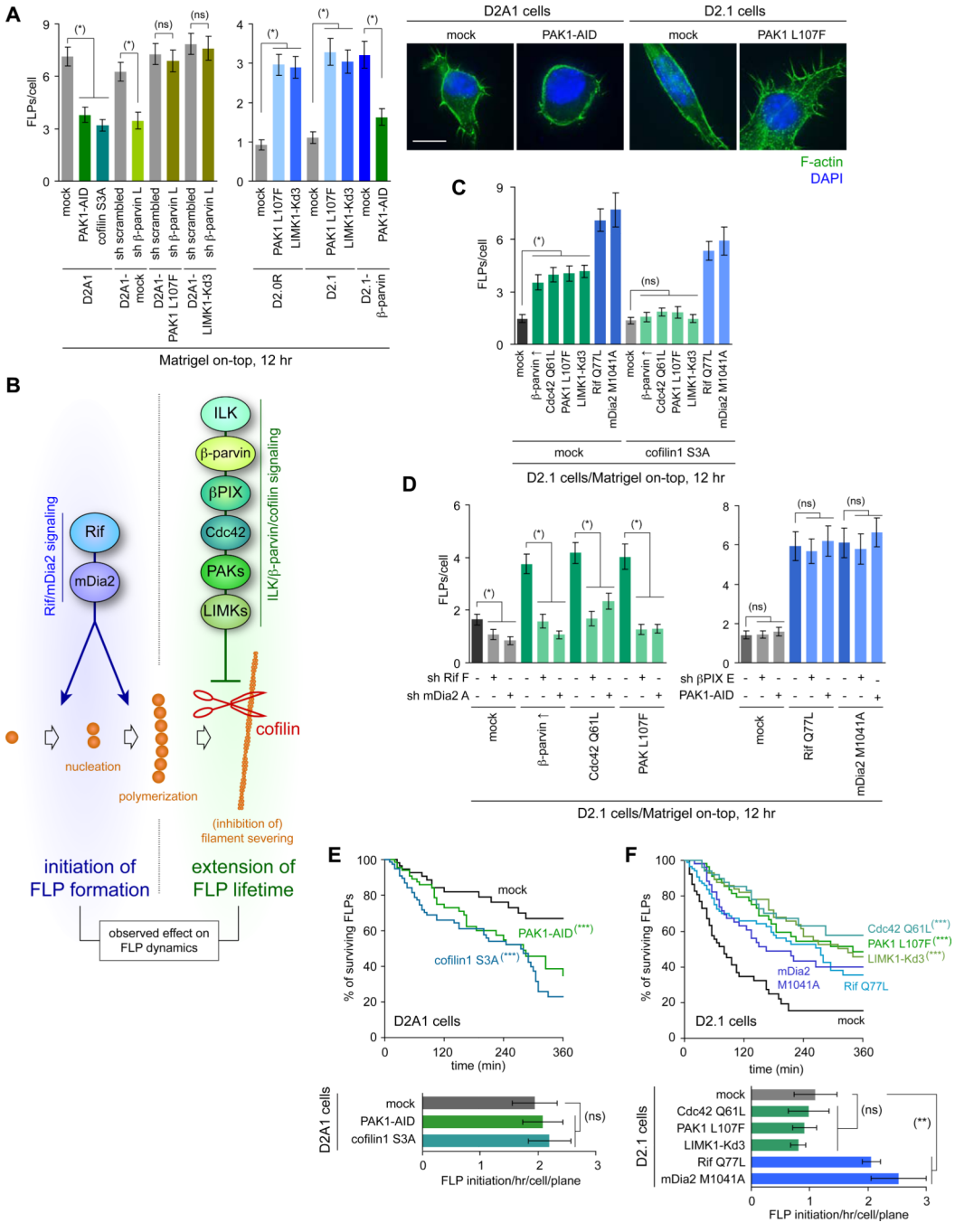

Figure 3. Cooperation of Rif/mDia2 and ILK/β-parvin/cofilin pathways in FLP regulation

(A) Role of PAK/LIMK/cofilin axis in FLP regulation. Cells manipulated as indicated to alter the activity of PAK/LIMK/cofilin signaling were analyzed for FLP formation in MoT cultures. Bar = 10 μm.

(B) Cooperation of the two signaling axes, Rif/mDia2 and ILK/β-parvin/cofilin, for abundant FLP display.

(C) Differential requirement for cofilin inactivation between Rif/mDia2 and ILK/β-parvin/cofilin signaling pathways. The control (mock) and cofilin1 S3A-expressing D2.1 cells were

further engineered to activate either of Rif/mDia2 or ILK/β-parvin/cofilin signaling pathways and analyzed for FLP formation.

(D) Requirement for basal Rif/mDia2 activity in β-parvin/PAK-driven FLP formation. The D2.1 cells with enforced activation of ILK/β-parvin/cofilin signaling were further engineered to knockdown Rif or mDia2 expression (left), while those with enforced Rif/mDia2 activation were additionally engineered to knockdown βPIX or to overexpress PAK1-AID (right), before the FLP formation by these cells was analyzed.

(E, F) Effects of signaling manipulation on FLP dynamics. D2A1 (E) and D2.1 (F) cells (expressing lifeact-YPet) were engineered to block and stimulate FLP formation, respectively, and analyzed by time-lapse microscopy. See also Movies S6–S8.

Values = means ± SEM (n = 100: A, C, D; $n \fallingdotseq 20$: E, F). (*) $p < 0.0001$, (**) $p < 0.05$, (ns) $p > 0.2$ (by Student's t-test). (***) $p < 0.0001$ (vs mock; by log-rank test). See also Figure S3.

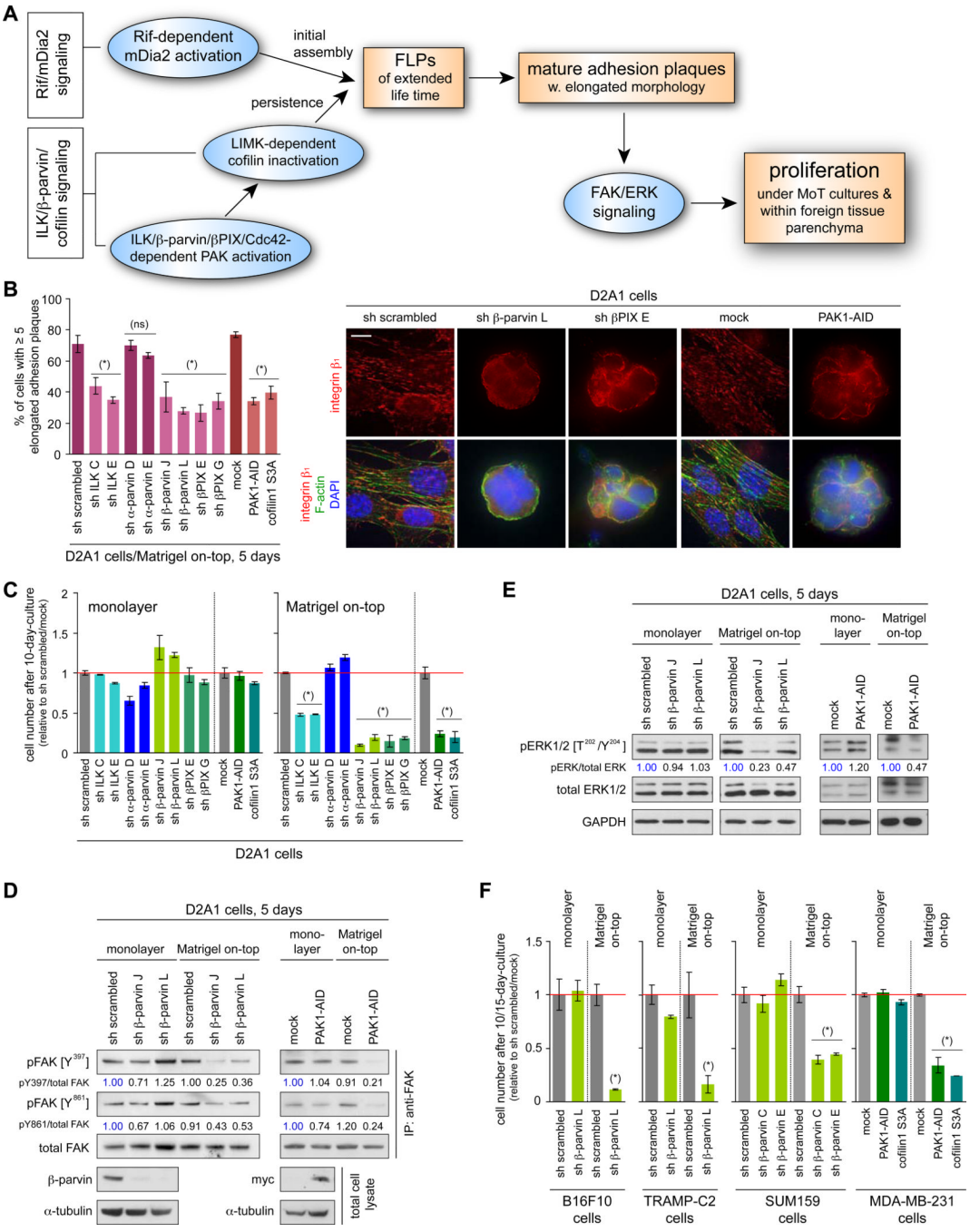

Figure 4. *in vitro* effects of ILK/β-parvin/cofilin signaling manipulation

(A) Cell-biological and biochemical events that drive cell proliferation in MoT culture and within the lung parenchyma.

(B, C) Role of ILK/β-parvin/cofilin signaling in adhesion plaque assembly and proliferation. The D2A1 cells were manipulated as indicated, with which the rate of mature adhesion plaque assembly in MoT culture (B) and the cell numbers after 10 days of monolayer or MoT culture (C) were determined. Bar = 10 μm.

(D, E) β-parvin/PAK signaling and FAK/ERK activation. Values represent the intensities of pFAK (pERK) bands relative to that of the corresponding total FAK (ERK) band.

(F) ILK/β-parvin/cofilin signaling and proliferation in various cell types. Indicated cell types were manipulated to block ILK/β-parvin/cofilin signaling, with which the cell numbers after 10 (15 for MDA-MB-231) days of monolayer/MoT cultures were determined.
Values = means ± SD (*n* = 3: B, C, F). (*) $p < 0.02$, (ns) $p > 0.1$ (vs sh scrambled/mock).
See also Figure S4.

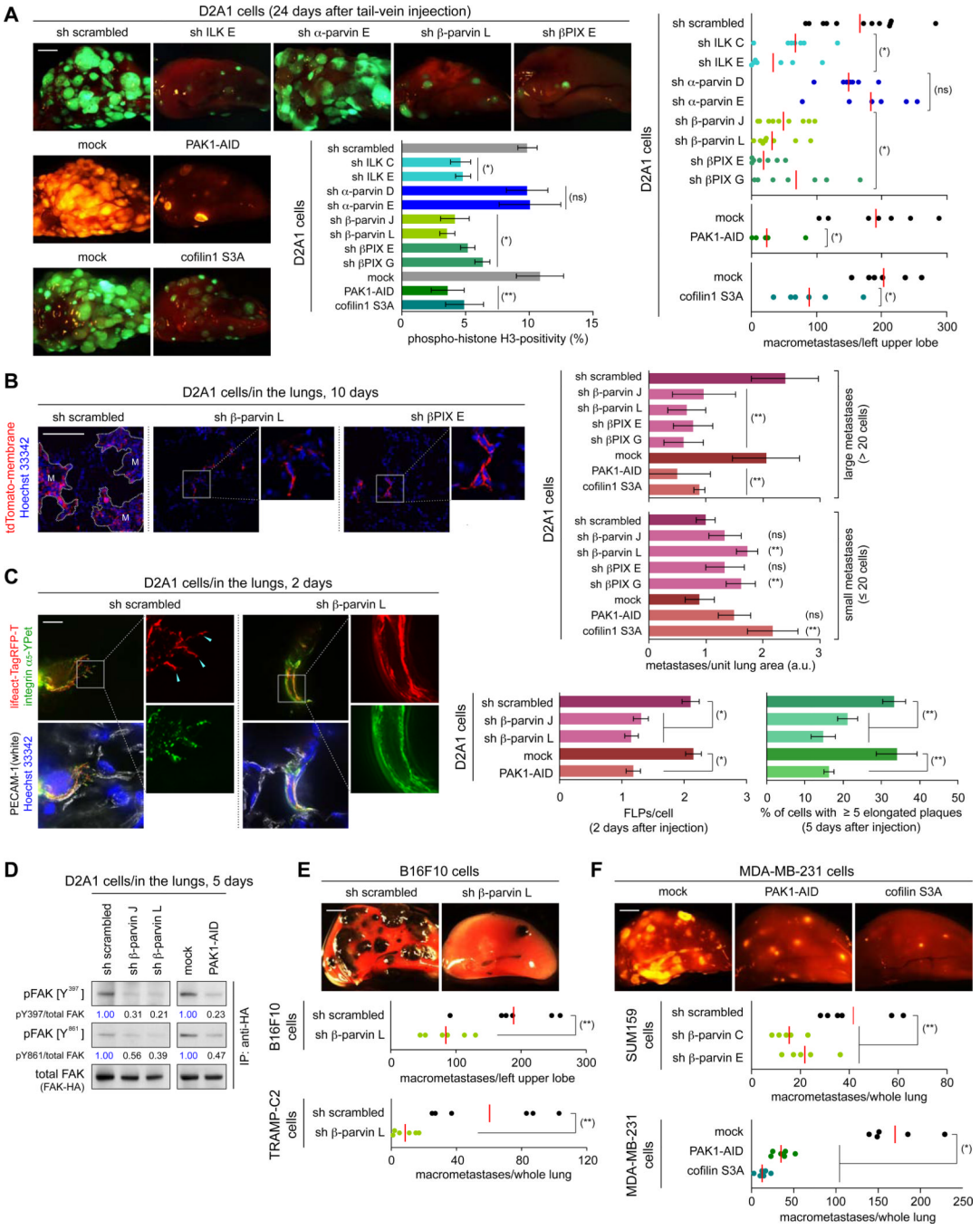

Figure 5. *in vivo* effects of ILK/β-parvin/cofilin signaling manipulation

(A, B) ILK/β-parvin/cofilin signaling and metastatic colonization. The D2A1 cells expressing fluorescent markers (GFP or tdTomato; A, tdTomato-membrane; B) were manipulated as indicated and tail-vein injected. In A, representative lung images (left) and the numbers of macrometastases (right) 24 days after injection, as well as the phospho-histone H3 positivity of the cells residing in the lungs 7 days after injection (middle), were presented. Here and in E, F, the red bar represents the mean value within each sample group. In B, relative numbers of small (≤ 20 cells) and large metastases (> 20 cells) were quantified on the lung sections prepared 10 days after injection. M = large metastases.

(C, D) β-parvin/PAK axis and *in vivo* cell-matrix adhesions. In C, the D2A1 cells expressing integrin α_5-YPet (green) and lifeact-Tag-RFP-T (red), further engineered as indicated, were tail-vein injected. FLP formation was analyzed on the lung sections, where blood vessels (PECAM-1; white) and nuclei (Hoechst 33342; blue) were also visualized (left/middle). The formation of elongated adhesion plaques was scored similarly, except for using α-actinin-Tag-RFP-T fusion protein instead of lifeact-Tag-RFP-T (right). In D, the D2A1 cells engineered as indicated, also expressing FAK-HA, were tail-vein injected. 5 days later, FAK-HA was immunoprecipitated from the lung lysate and analyzed by immunoblotting.
(E, F) Role of ILK/β-parvin/cofilin signaling in lung colonization by various cell types. The control and manipulated B16F10, TRAMP-C2, SUM159 and MDA-MB-231 cells, also expressing GFP (E) or tdTomato (F), were tail-vein injected and subsequent formation of lung metastases was analyzed.
Values = means ± SD (*n* = 3: A [middle], B, C [right]); means ± SEM (*n* = 150: C [left]). Bars = 2 mm (A, E, F), 100 μm (B), 10 μm (C). (*) $p < 0.005$, (**) $p < 0.05$, (ns) $p > 0.05$ (vs sh scrambled/mock). See also Figure S5.

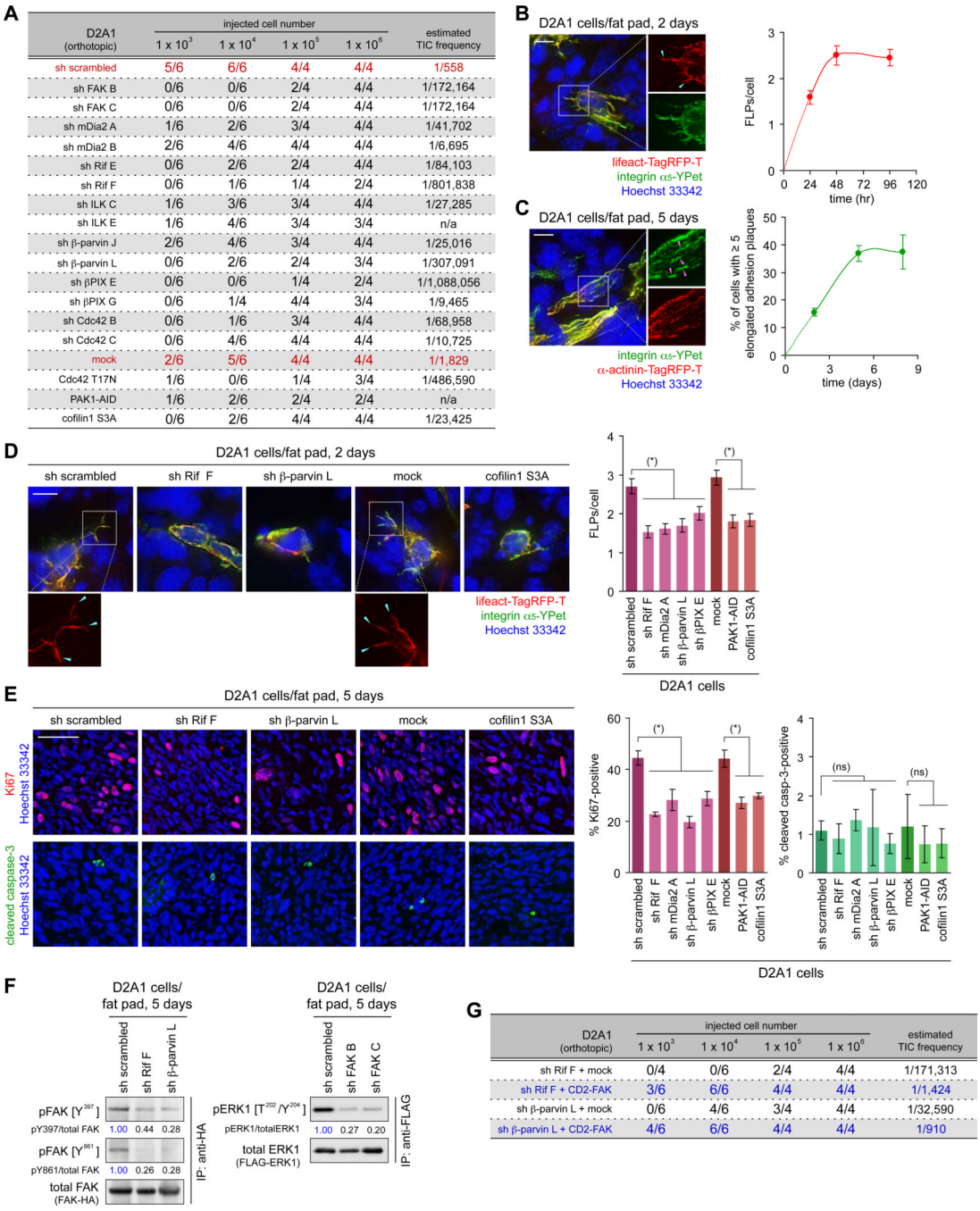

D2A1 (orthotopic)	injected cell number 1 x 10^3	1 x 10^4	1 x 10^5	1 x 10^6	estimated TIC frequency
sh scrambled	5/6	6/6	4/4	4/4	1/558
sh FAK B	0/6	0/6	2/4	4/4	1/172,164
sh FAK C	0/6	0/6	2/4	4/4	1/172,164
sh mDia2 A	1/6	2/6	3/4	4/4	1/41,702
sh mDia2 B	2/6	4/6	4/4	4/4	1/6,695
sh Rif E	0/6	2/6	2/4	4/4	1/84,103
sh Rif F	0/6	1/6	1/4	2/4	1/801,838
sh ILK C	1/6	3/6	3/4	4/4	1/27,285
sh ILK E	1/6	4/6	3/4	3/4	n/a
sh β-parvin J	2/6	4/6	3/4	4/4	1/25,016
sh β-parvin L	0/6	2/6	2/4	3/4	1/307,091
sh βPIX E	0/6	0/6	1/4	2/4	1/1,088,056
sh βPIX G	0/6	1/4	4/4	3/4	1/9,465
sh Cdc42 B	0/6	1/6	3/4	4/4	1/68,958
sh Cdc42 C	0/6	4/6	4/4	4/4	1/10,725
mock	2/6	5/6	4/4	4/4	1/1,829
Cdc42 T17N	1/6	0/6	1/4	3/4	1/486,590
PAK1-AID	1/6	2/6	2/4	2/4	n/a
cofilin1 S3A	0/6	2/6	4/4	4/4	1/23,425

D2A1 (orthotopic)	injected cell number 1 x 10^3	1 x 10^4	1 x 10^5	1 x 10^6	estimated TIC frequency
sh Rif F + mock	0/4	0/6	2/4	4/4	1/171,313
sh Rif F + CD2-FAK	3/6	6/6	4/4	4/4	1/1,424
sh β-parvin L + mock	0/6	4/6	3/4	4/4	1/32,590
sh β-parvin L + CD2-FAK	4/6	6/6	4/4	4/4	1/910

Figure 6. FLP formation and tumorigenesis of experimentally-implanted cells

(A) Role of FLP-regulating proteins in primary tumor formation. The D2A1 cells were engineered as indicated and implanted into the mammary fat pads. 28 days later, the formation of palpable tumors was scored, from which TIC frequency was calculated.

(B, C) FLPs and elongated adhesion plaques formed by the mammary fat pad-implanted cells. The D2A1 cells expressing integrin α_5-YPet (green) and either of the lifeact-Tag-RFP-T (red; B) or α-actinin-Tag-RFP-T (red; C) were implanted, together with non-labeled D2A1 cells. The formation of FLPs (blue arrowheads; B) and elongated adhesion plaques (pink arrowheads; C) was analyzed on the sections of the fat pads.

(D, E) Effect of blocking FLP formation in the mammary fat pad-implanted cells. In D, fluorescent-labeled and non-labeled D2A1 cells, further manipulated as indicated, were mixed and implanted to analyze FLP formation within the mammary fat pads. In E, D2A1 cells were engineered as indicated and implanted. Proliferation and apoptosis of implanted cells were analyzed by staining the sections of the fat pads for Ki67 (red) and cleaved caspase-3 (green), respectively.
(F) FAK/ERK activation in the mammary fat pad-implanted cells. The D2A1 cells expressing either of FAK-HA or FLAG-ERK1 were further manipulated as indicated and implanted. Subsequently, FAK-HA or FLAG-ERK1 was immunoprecipitated from the lysate of the fat pads and analyzed.
(G) Restoring tumor-initiating ability by enforced FAK activation. The D2A1 cells with Rif or β-parvin knockdown were further manipulated to express the constitutively active CD2-FAK. Primary tumor formation by these and the control cells was analyzed. Bars = 10 μm (B-D), 100 μm (E). (*) $p < 0.01$, (ns) $p > 0.1$. See also Figure S6.

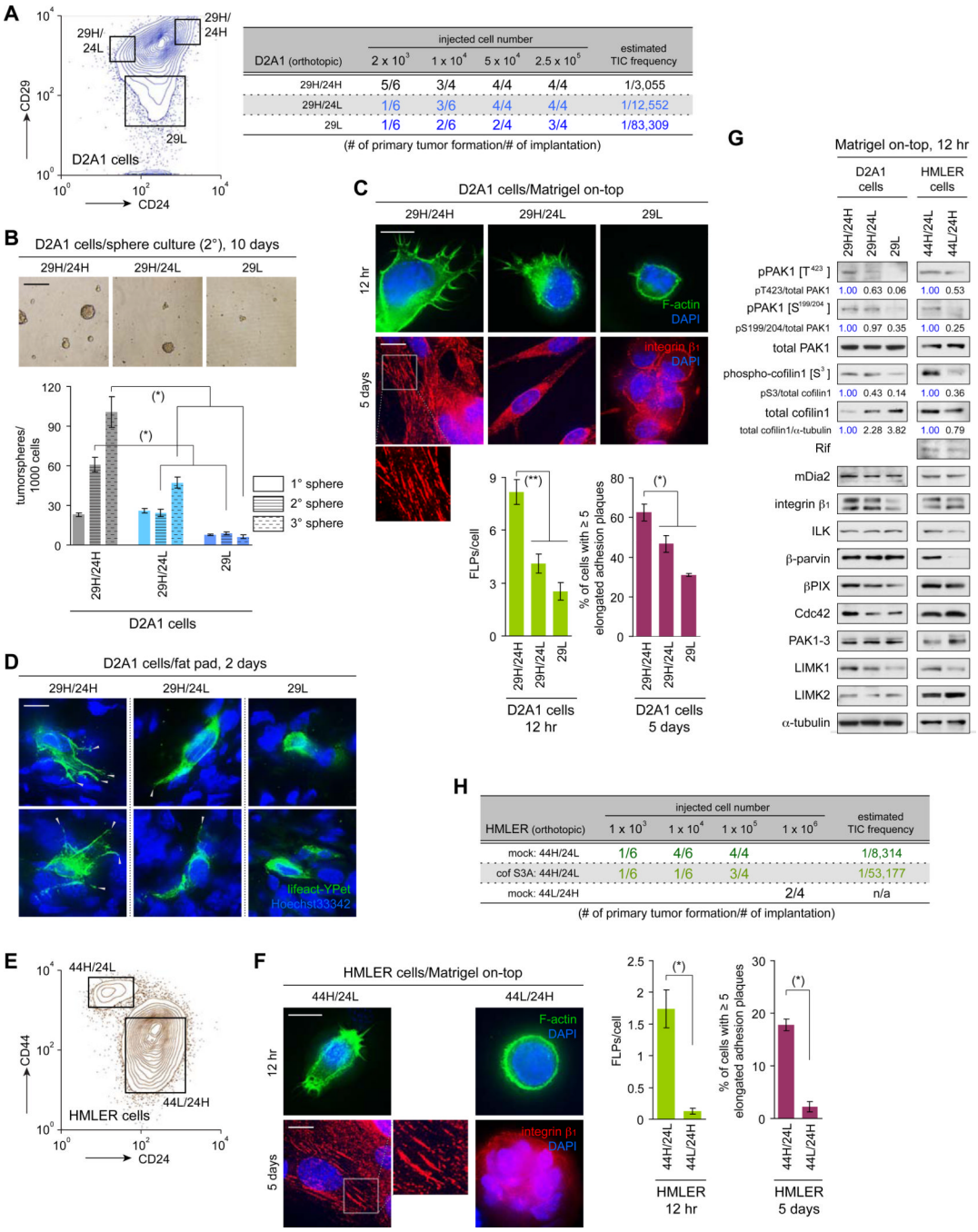

Figure 7. Display of abundant FLPs by cells of the TIC-enriched subpopulation

(A) Sorting of the D2A1 cells by CD29/CD24 expression. The cells of each subpopulation were implanted into mammary fad pads to score primary tumor formation (right).

(B) Tumor sphere formation by the sorted D2A1 cells. Cells were sequentially passaged for the 3 rounds of 10-day culture. The numbers of tumorspheres after each round of culture were scored (bottom). Representative images of cells after the 2nd round of culture are also presented (top).

(C, D) Formation of FLPs and elongated adhesion plaques by the sorted D2A1 cells. In C, sorted D2A1 cells were propagated in MoT cultures to analyze FLP/elongated adhesion

plaque formation. In D, the D2A1 cells that did and did not express the fluorescent actin marker lifeact-YPet (green) were sorted, mixed and implanted. The formation of FLPs (gray arrowheads) by these cells was analyzed on the sections of the fat pads.

(E) Sorting of the HMLER cells by CD44/CD24 expression.

(F) Formation of FLPs and elongated adhesion plaques by the sorted HMLER cells in MoT cultures.

(G) Expression of FLP-regulating proteins in cells of the various D2A1 and HMLER subpopulations. Cells of these subpopulations were propagated in MoT cultures and analyzed by immunoblotting.

(H) Blocking ILK/β-parvin/cofilin signaling in the 44H/24L subpopulation of HMLER cells. HMLER cells were manipulated to express constitutively active cofilin1 S3A. These and the control cells were sorted and 44H/24L subpopulation obtained from each cell type was implanted to score primary tumor formation.

Values = means ± SD (*n* = 3: B, C [right], F [right]); means ± SEM (*n* = 100: C [left], F [left]). Bars = 200 μm (B), 10 μm (C, D, F). (*) $p < 0.005$, (**) $p < 0.02$. See also Figure S7.

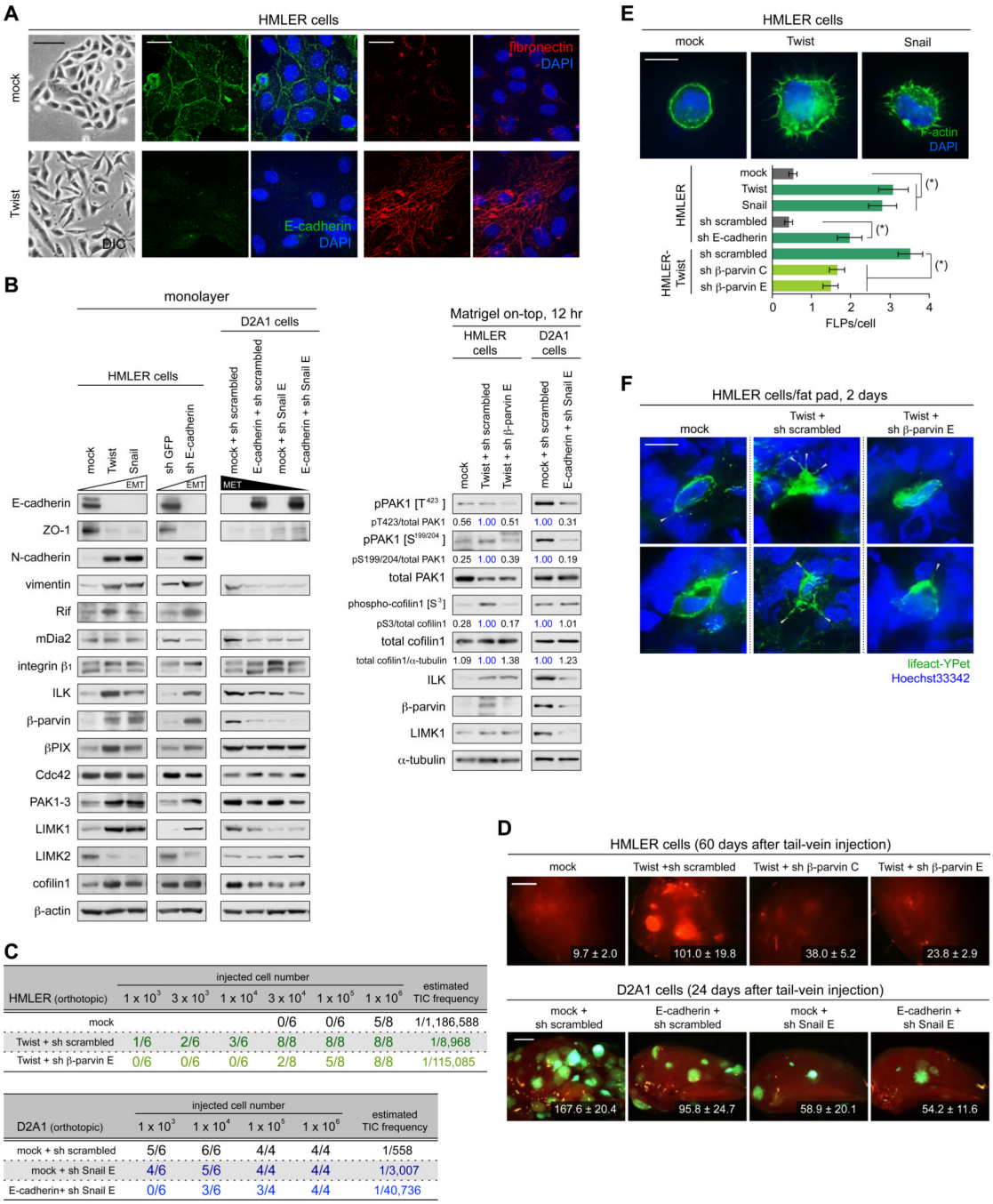

C

HMLER (orthotopic)	injected cell number 1 x 10^3	3 x 10^3	1 x 10^4	3 x 10^4	1 x 10^5	1 x 10^6	estimated TIC frequency
mock				0/6	0/6	5/8	1/1,186,588
Twist + sh scrambled	1/6	2/6	3/6	8/8	8/8	8/8	1/8,968
Twist + sh β-parvin E	0/6	0/6	0/6	2/8	5/8	8/8	1/115,085

D2A1 (orthotopic)	injected cell number 1 x 10^3	1 x 10^4	1 x 10^5	1 x 10^6	estimated TIC frequency
mock + sh scrambled	5/6	6/6	4/4	4/4	1/558
mock + sh Snail E	4/6	5/6	4/4	4/4	1/3,007
E-cadherin+ sh Snail E	0/6	3/6	3/4	4/4	1/40,736

Figure 8. Functional connection between FLP formation and EMT program

(A) Twist-induced EMT in the HMLER cells. The control (mock) and Twist-expressing HMLER cells were propagated as a monolayer and stained for E-cadherin (green), fibronectin (red) and the nuclei (blue) (right). Differential interference contrast (DIC) images of these cells are also presented (left).

(B) Changes in the expression levels of EMT-markers and FLP-regulators. HMLER cells and D2A1 cells were engineered as indicated to undergo an EMT and MET, respectively. These and the control cells were propagated either as a monolayer (left) or in MoT cultures (right) and analyzed by immunoblotting.

(C, D) Effect of EMT/MET on primary tumor formation and metastatic colonization. In C, indicated cell types were mammary fat pad-implanted and primary tumor formation was scored. In D, indicated cells types, also expressing GFP or tdTomato, were tail-vein injected to score metastasis formation in the lungs. The numbers of macrometastases observed on the surface of the entire lungs (HMLER) or left upper lobe of the lungs (D2A1) are presented.
(E, F) FLP formation before and after EMT induction. In E, the HMLER cells engineered as indicated were analyzed for FLP formation in MoT culture. (*) $p < 1 \times 10^{-5}$. In F, HMLER cells engineered as indicated were further manipulated to express lifeact-YPet. These and non-labeled cells were mixed and fad pad-implanted to score the formation of FLPs (gray arrowheads).
Values = means ± SEM ($n \geq 5$: D, $n = 100$: E). Bars = 100 μm (A [left]), 20 μm (A [right]), 2 mm (D), 10 μm (E, F). See also Figure S8.